ELSEVIER

Journal of Wind Engineering
and Industrial Aerodynamics 83 (1999) 95–107

JOURNAL OF wind engineering AND industrial aerodynamics

www.elsevier.com/locate/jweia

A wind tunnel study of turbulent flow over a three-dimensional steep hill

Takeshi Ishihara*, Kazuki Hibi, Susumu Oikawa

Environmental Engineering Department, Institute of Technology, Shimizu Corporation, 3-4-17, Etchujima, Koto-ku, Tokyo 135-8530, Japan

Abstract

The turbulent flow over a circular hill, having a cosine-squared cross section and a maximum slope of about 32°, was investigated using split-fiber probes designed for measuring flows with a high turbulence and separation. Profiles of the means and variances for the three velocity components are presented and compared with those in the undisturbed (no-hill) boundary layer. The turbulent boundary layer separated behind the crest and reattached just at the lee foot of the hill. The pronounced speed-up of flow occurs not only at the hilltop but also at the midway slope on its side. The maximum perturbations in the longitudinal and vertical velocity variances were observed at the height of the hill ($z/h = 1$), corresponding to the separated recirculating flow on the lee slope of the hill, while the maximum in the lateral velocity variance appeared at the height of $z/h = 0.125$ beyond the hill, corresponding to the low-frequency motion in the wall layer.

Keywords: Three-dimensional steep hill; Split-fiber measurements; Mean flow; Turbulence statistics; Separation; Low-frequency motion

1. Introduction

Over the last two decades, turbulent flow over hills has often been studied, because of its importance in a wide range of subjects, such as the safety of structures, extraction of wind energy, pollutant dispersion, wind damage to agriculture and forestry, and aviation safety. Reviews of recent developments which focus on neutrally stratified turbulent flow over topography were covered by Taylor et al. [1] and Finnigan [2].

* Corresponding author. Fax: + 81-3-3643-7260.
E-mail address: meng@sit.shimz.co.jp (T. Ishihara)

0167-6105/99/$ - see front matter
PII: S0167-6105(99)00064-1

These reviews provide some understanding of how a specified upwind mean flow and turbulence should be modified on passing over low hills with a moderate slope. Detailed quantitative information on the mean flow and turbulence structures behind three-dimensional steep hills is lacking, although some field and wind tunnel studies of flow over three-dimensional isolated hills have been conducted; see, for example, [3–8].

In the current study, we applied split-fiber probes to measure three velocity components in order to provide details of mean flow and turbulence statistics over a three-dimensional steep hill, and shed some light on the structure and dynamics of the turbulent flow in the near-wake region behind three-dimensional steep hills.

2. Experimental details

2.1. Facility

The present study was conducted in a return wind tunnel, which has a working section of 1.1 m wide, 0.9 m high and 7 m long. The free-stream turbulence intensity is about 0.5% at the first measurement location. A neutrally stratified atmospheric boundary layer was simulated, using two 60 mm high cubic arrays placed just downstream of the contraction exit and followed by 20 and 10 mm cubic roughness element, covering 1.2 m of the test-section floor. The remaining 5.8 m of the test-section floor was covered with plywood, which was relatively as smooth as the hill surface, to avoid the complication of rough to smooth transition. The wind speed outside the boundary layer U_∞ was monitored throughout the experiment using a Pitot tube and maintained at 5.8 m/s. The resulting boundary layer was about 0.36 m thick at the point where the hill was mounted (4.6 m downstream of the contraction exit) and the scale of the simulated boundary layer was about 1 : 1000 of the atmospheric boundary layer, on the basis of the power spectra of the longitudinal velocity component. The simulated boundary layer had a Reynolds number, $U_\infty \delta/\nu$, of 1.4×10^5, and the surface Reynolds number, $u_* z_0/\nu$, was about 0.14. This implies that the flow was not quite aerodynamically rough and hence slightly dependent on Reynolds number. However, it will differ from fully aerodynamically rough flow only very close to the surface.

The model hill was machined from wood and had the shape $z_s(x, y) = h\cos^2(\pi(x^2 + y^2)^{1/2}/2L)$ with $h = 40$ mm and $L = 100$ mm. The maximum slope was thus about 32°. Fig. 1 shows details of the hill and coordinate system used in the study, where x, y and z are the free-steam, spanwise and vertical directions, respectively. In the x-coordinate, zero is the center of hill (4.6 m downstream of the contraction exit). A second vertical coordinate, $z' = z - z_s(x, y)$, is also used to denote height above the local surface.

2.2. Measurement techniques

Velocity measurements in the undisturbed boundary layer were made using constant temperature hot-wire anemometers (DANTEC 56C01 and 56C17) with

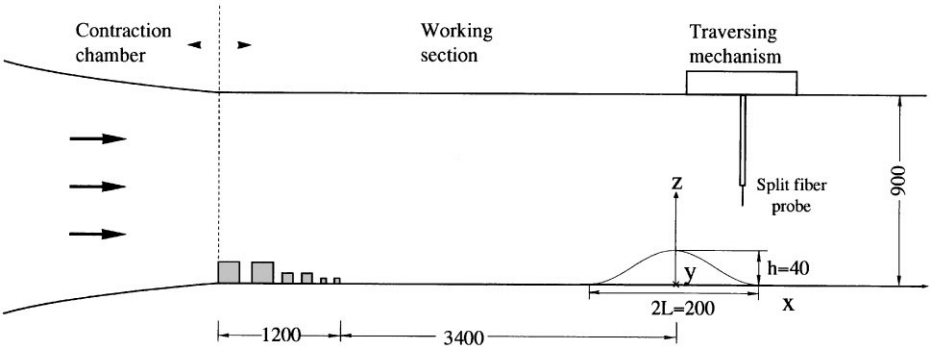

Fig. 1. Sketch defining the notations used in this study.

cross-wire probes (55R53 and 55R54). The X-wires were calibrated against a Pitot tube in the free stream, using the relation $U = aE^3 + bE^2 + cE + d$, where U is the velocity, E is the voltage, and a, b, c and d are constants. A least-squares fitting procedure was used, and calibration data differed from the final fit by less than 1%. The drifts in calibration coefficients were very small, since temperature in the tunnel was fixed during data acquisition.

Since X-wire probe anemometers for turbulence measurement cannot give reasonable accuracy when the turbulence intensity is larger than 0.3 [9], all velocity measurements around the hill were made with two kinds of split-fiber probes. One, 55R55 straight probe, had sensors perpendicular to the probe axis and was set to have the plane of split normal to the free stream. Thus, it was able to detect reversals of the local flow direction and used to measure the longitudinal velocity component. The other, 55R57 90° probe, had sensors parallel to the probe axis and was set to have the plane of split parallel to the free stream to measure the spanwise and vertical velocity components. Split-fiber probes have been used for investigating the structure of a turbulent separation bubble as reported by Kiya and Sasaki [10]. The calibration procedures of split-fiber probes have been described by Sasaki and Kiya [11] for air flows and by Boerner and Leutheusser [12] for bubbly water/air flows, and modified by the authors [13]. In this method, output voltages from the anemometers connected to the two films were compared with each other, and since the output from one anemometer is greater than that of the other, the instantaneous flow direction can be determined. For accurate results the overheat ratios of the two films must be closely matched. Fig. 2 shows the tip of a type 55R55 split-fiber probe. The sensors are nickel thin-films deposited on a 200 μm quartz fiber with an active length of 1.2 mm and are covered with an approx. 0.5 μm thick quartz coating to protect against oxidation. Split width is approx. 0.03 mm.

In order to measure one component of a velocity vector as defined in Fig. 2, two calibration functions for, respectively, the magnitude of the velocity vector normal to the axis of the fiber, U_N, and the pitch angle, θ, are required. For the U_N, it can be

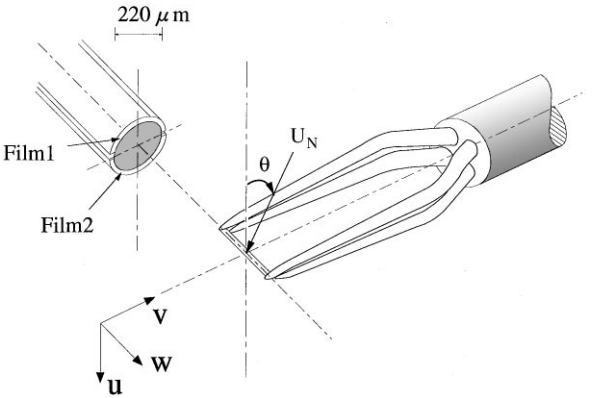

Fig. 2. Tip of a type 55R55 split-fiber probe.

described as a function of the sum of the outputs of the two films and is given by

$$U_N = f(E_1 + E_2), \tag{1}$$

where E_1 and E_2 denote voltages obtained from the two films, which are set at zero using two differential amplifier circuits when no free stream exists, and f represents a cubic spline function. Split-fiber probes were calibrated against a Pitot tube and a Draft master (Kanomax model 6311) which was used as the free-stream velocity was less than 1 m/s. As expected, the sum of the outputs of the two films is practically independent of the pitch angle. The variation of U_N with the pitch angle obtained in $U_\infty = 2$ and 6 m/s was less than $\pm 1.5\%$.

The difference in the outputs of the two films, $\Delta E = E_1 - E_2$, can be described by a function of the pitch angle θ with U_N as a parameter and expressed as

$$\Delta E = g(\theta)\Delta E_{max}(U_N). \tag{2}$$

In this, g is the required empirical calibration function, and $\Delta E_{max}(U_N)$ is the maximum difference in the output of the two films. For practical application, g is generally presented in the cosine form. Thus, the pitch angle θ is given by

$$\theta = \begin{cases} \cos^{-1}(\Delta E/\Delta E_0) & E_1 \geqslant E_2, \\ \cos^{-1}(\Delta E/|\Delta E_{180}|), & E_1 < E_2, \end{cases} \tag{3}$$

where ΔE_0 and ΔE_{180} are the differences in the output of the two films according to the pitch angle θ of 0° and 180°, and variations of them with U_N are described by two cubic spline functions.

The calibrations were performed by rotating the probe in smooth uniform flow. Pitch is defined as the rotation around the sensor films axes, yaw as the rotation around the axis normal to the sensor axes. The final calibration results are shown in Fig. 3. The ideal cosine response is drawn on the figures as a solid lines. The mean directional responses for pitch and yaw are favorably close to the ideal cosine form.

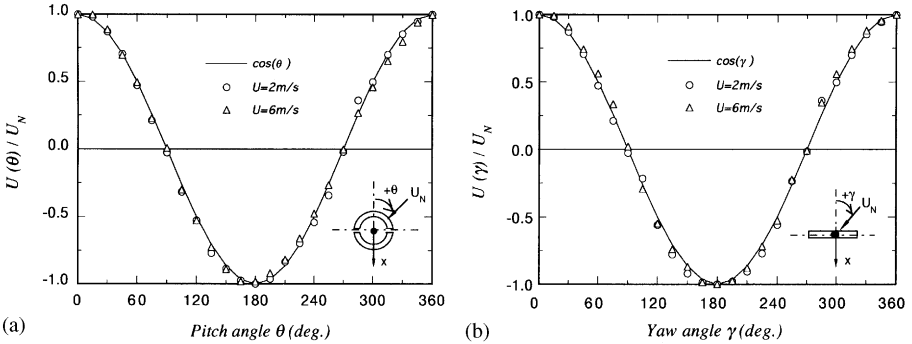

Fig. 3. Calibration in uniform flow: (a) pitch; (b) yaw.

The response of the split-fiber probes was checked by comparing measured u-spectra with those obtained by the single hot-wire probe in $U_\infty = 2$ and 6 m/s. The spectra were practically identical for frequencies less than 1 kHz. In all of our measurements, the analog voltages were low-pass filtered in 1 kHz and digitized in a sampling rate of 2 kHz. A sampling time of 60 s was used for mean velocities and turbulence statistics.

3. Results and discussion

3.1. Flow characteristics in the undisturbed boundary layer

Fig. 4a shows the profile of mean velocity U at the positions $x/h = 0$ (4.6 m downstream of the contraction exit). The velocity profile is adequately represented by a logarithmic law, $U/u_* = k^{-1} \ln(z/z_0)$ with $u_* = 0.212$ m/s and $z_0 = 0.01$ mm, in the surface layer and by a power law, $U/U_{\text{ref}} = (z/z_{\text{ref}})^n$, with an exponent $n = 0.135$ through most of the boundary layer. Considering that the simulated boundary layer has a scale of 1/1000, the equivalent full scale z_0 is 0.01 m, which is characteristic of a grass or heather covered hill like Blasheval [4].

Turbulence profiles, σ_u, σ_v and σ_w, at the same downstream position are plotted in Fig. 4b. They are similar in shape to those obtained by Arya and Gadiyaram [7]. The near-surface ratios, σ_u/u_*, σ_v/u_* and σ_w/u_*, have values of approximately 2.4, 1.6 and 0.8, respectively, in reasonable accordance with those obtained in other wind tunnel studies, for example, Gong and Ibbetson's values [8] of 2.2, 1.5 and 1.0, or Counihan [14] of 2.5, 1.9 and 1.3 for the atmospheric surface layer.

The lateral uniformity of the flow was checked at two heights, 0.25 h and 1 h at the future location of the hill. The variations were about $\pm 1\%$ in the mean velocity components, $\pm 2.5\%$ in the normal stress components.

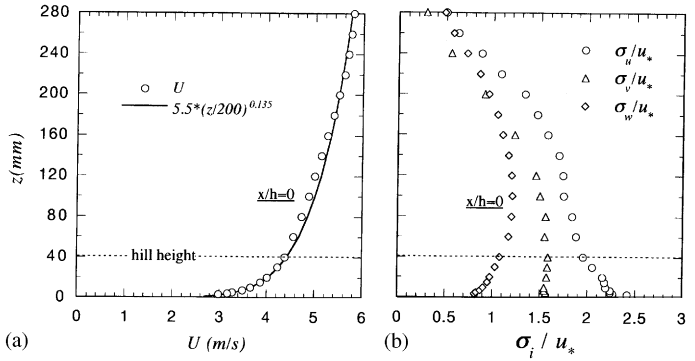

Fig. 4. Variation of mean velocity and three normal stress components with height z over the flat floor at the location $x/h = 0$: (a) mean velocity; (b) three normal stress components.

3.2. *Mean flow field*

Three velocity components were measured on the center line of the hill and at various positions on the side of the hill. Fig. 5 shows profiles of mean velocity components of U and W measured on the center line of the hill with the profile in the undisturbed (no-hill) boundary layer (dashed line). The mean velocity components are normalized by the mean velocity U_h obtained at the hill height h in the undisturbed boundary layer. For comparison, both the data obtained from the split-fiber probes and the data from the X-wire are represented in Fig. 5. It is clear that the X-wire gives unreasonable results in the near-wake region, as it is unable to differentiate between positive and negative quantities.

The most striking features of the longitudinal mean velocity U (see Fig. 5a) are the increase in velocity near the surface on top of the hill, the slight deceleration at the upwind hill foot, and the flow separation behind the hill. The vertical mean velocity W as shown in Fig. 5b is directed upward on the upstream side of the hill, and reaches a measured maximum of approximately $0.285U_h$ at $x/h = -0.625$. On the lee side of the hill, descending flow is observed above the separation bubble and the maximum negative value of about $-0.145U_h$ appears at $x/h = 1.875$. The v-component mean velocity (not shown here) is zero everywhere to well within the experimental uncertainty.

Fig. 6 illustrates the mean velocity vectors over the hill. The mean flow separates on the lee slope near the hill top, and reattaches just on the downwind hill foot. The dashed line in Fig. 6 is the locus of zero longitudinal velocity deduced from profiles like those in Fig. 5. Although the separation bubble is relatively shallow, the height of the bubble is slightly higher than that on the smooth cone reported by Castro and Snyder [5]. In the Castro and Snyder's experiment, the flow acceleration after the rough-to-smooth transition might help to prevent separation, since the smooth cone was mounted in rough terrain.

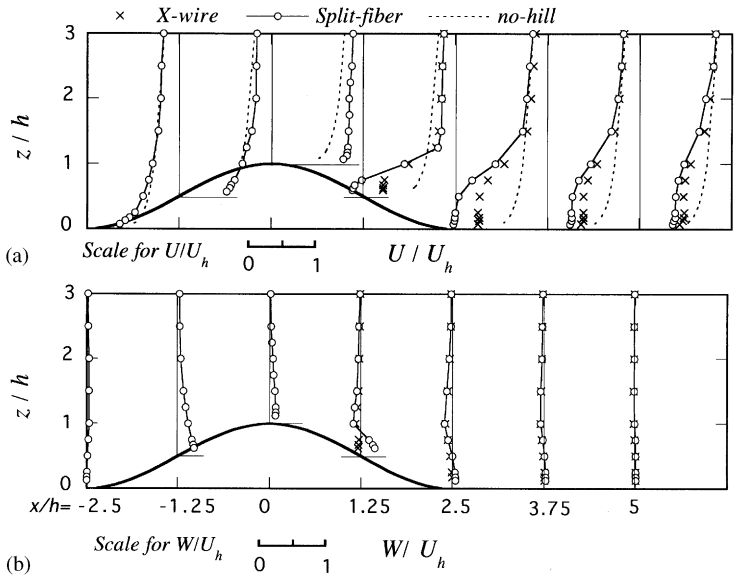

Fig. 5. Vertical profiles of (a) longitudinal and (b) vertical velocity components on the central plane of the hill. The profile in the undisturbed (no-hill) boundary layer is superimposed on the local profiles.

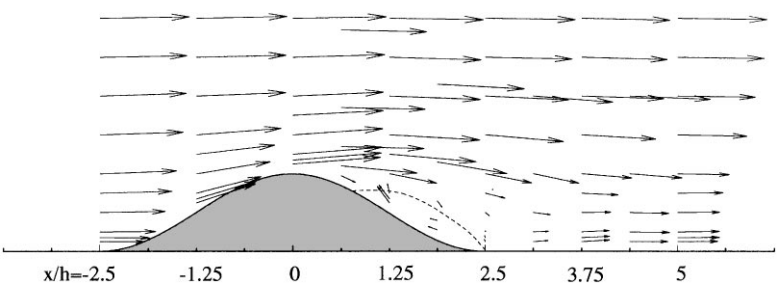

Fig. 6. Mean velocity U, W vectors in the central plane.

A few spanwise distributions of the longitudinal and lateral mean velocities at fixed $x/h = 3.75$ are shown in Fig. 7. Measurement were made in only half of the domain, assuming that the flow was symmetrical around the central plane. Although cross flows are weak at the height of the hill, relatively strong cross flows appear at a clearly off-center position in the region near the surface, and indicate low-level flow convergence in the near-wake region.

The mean speed-up on the hill holds an obvious interest for engineers interested in predicting wind loading on structures. Fig. 8 plots vertical profiles of the speed-up ratio, $S = U(z')/U_0(z')$, where the subscript "0" refers to the no-hill case. A reduction in

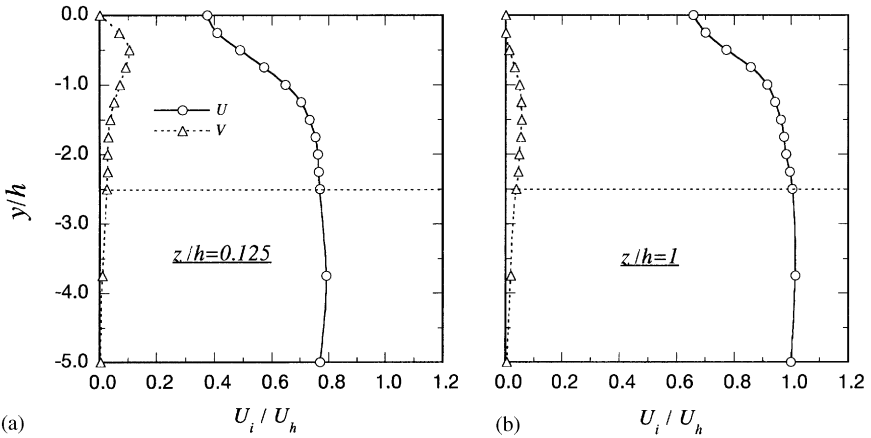

Fig. 7. Lateral distributions of the longitudinal and lateral velocity components behind the hill at (a) $x/h = 3.75$, $z/h = 0.125$ and (b) $x/h = 3.75$, $z/h = 1$.

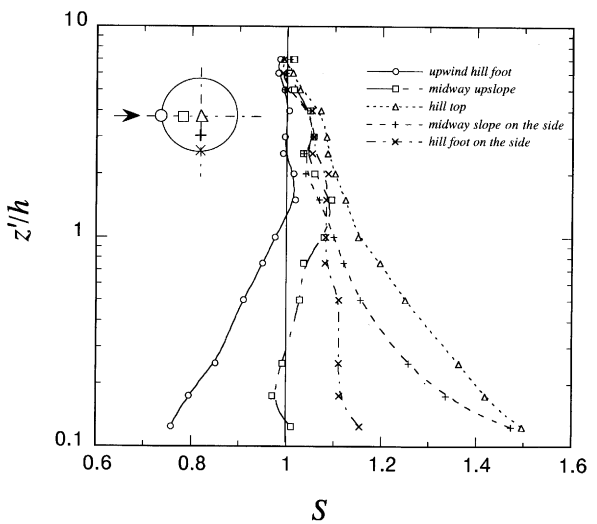

Fig. 8. Vertical profiles of the speed-up factor at several positions.

speed is observed at the upwind hill foot due to an upwind adverse pressure gradient. Over the hill, the flow accelerates and a speed-up ratio of 1.5 is observed at the height of $z'/h = 0.125$. This speed-up ratio is in reasonable accordance with Mason and King's value of 1.6 obtained at $z'/h = 0.13$ on Blasheval with a roughness length z_0 of 0.01 m. Our profile of speed-up ratio at the crest is also similar to that of Arya and Gadiyaram [7]. At the midway upwind slope, there is a negative speed-up at low levels and a positive speed-up at higher levels. On the side of the hill (on the $x = 0$

plane), it should be noted that a pronounced speed-up occurs at the midway slope, and decreases more rapidly with height than that above the crest. This feature has been observed by Hunt and Snyder [15] for their bell-shaped hill mounted in the thin boundary layer. The flow acceleration is also observed at the hill foot on the side.

3.3. Normal Reynolds stress field

Besides the mean velocity, it is of interest to know how turbulence might be modified as the flow goes over the hill. Turbulence structures behind a three-dimensional steep hill are poorly understood, although the longitudinal fluctuating velocity in the near-wake region behind a cone has been studied by Castro and Snyder [5] employing pulsed-wire anemometers.

Profiles of normal stress components, σ_u, σ_v and σ_w, are plotted in Fig. 9, which compares two sets of data measured by the split-fiber and X-wire probes. As

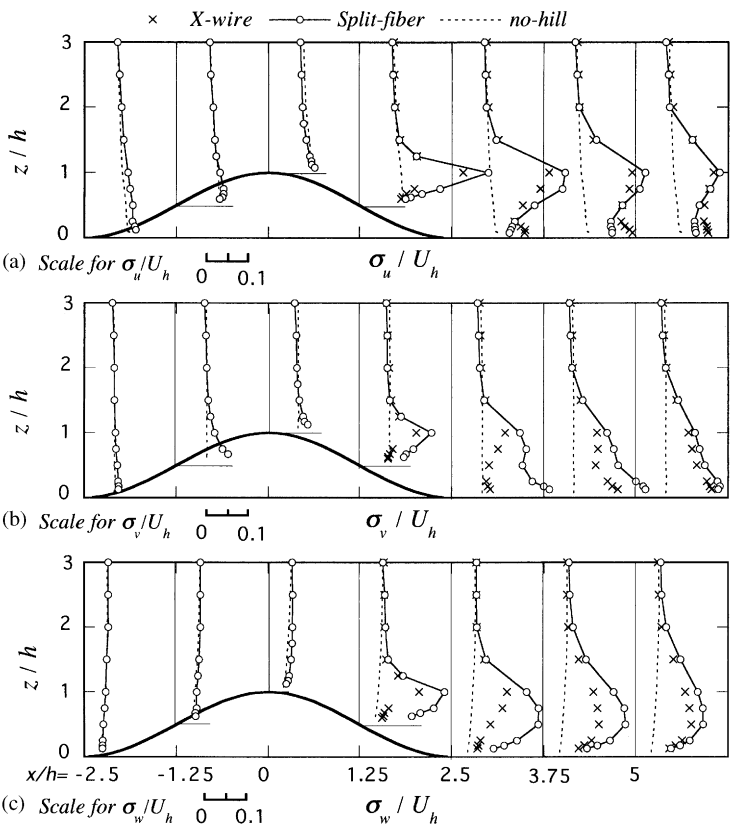

Fig. 9. Vertical profiles of three normal stress components on the central plane of the hill: (a) σ_u/U_h; (b) σ_v/U_h; (c) σ_w/U_h. The profiles in the undisturbed (no-hill) boundary layer is superimposed on the local profiles.

anticipated, the results obtained from the X-wire are lower than those from the split fiber in the near-wake region. This is because the X-wire underestimates lateral and vertical velocity components, when longitudinal velocity components are small. The X-wire results in the near-wake region are seen to be reliable only above the height of $z/h = 1.5$, where the local turbulence intensity, σ_u/U, is less than 0.3.

Relative to upwind, σ_u and σ_v display some increase at low levels from the upwind deceleration region to the hilltop, while the increase in σ_w is very slight. In the lee slope of the hill, all three normal stress components show strong peaks around the regions of maximum shear in the longitudinal velocity profiles. It is clear that these highly turbulent energies are generated by the flow separated on the lee slope of the hill and far in excess of those that occur in the undisturbed boundary layer. Maximum values of σ_u/U_h, σ_v/U_h and σ_w/U_h are 0.32, 0.18 and 0.21 respectively, roughly in accordance with those obtained by Kiya and Sasaki [10] with their values of 0.25, 0.17 and 0.22 for the separation bubble formed along the sides of a blunt flat plate. In the near-wake region beyond the hill, σ_u and σ_w show clear peaks and decay gradually with distance behind the hill. The heights corresponding to the peaks are close to 1 h for σ_u and 0.5 h for σ_w. These features have been observed by Arya and Gadiyaram [7] for their 26.6° cone in the far-wake region. The most striking behavior in the three-dimensional wake is that σ_v profiles show second local maxima in the so-called wall layer, which could not be observed in the typical two-dimensional wake as described by Castro and Haque [16] and Itoh and Kasagi [17]. In this layer, the σ_u profiles show a roughly constant value. Castro and Snyder [5] seem to observe this constant σ_u layer, although they accord it little attention in their paper.

Fig. 10 shows a few lateral distributions of three normal stress components at $x/h = 3.75$. At the height of $z/h = 1$, it is clear that the separation behind the crest of the hill has a dominat influence on the flow. The three normal stresses show maximum

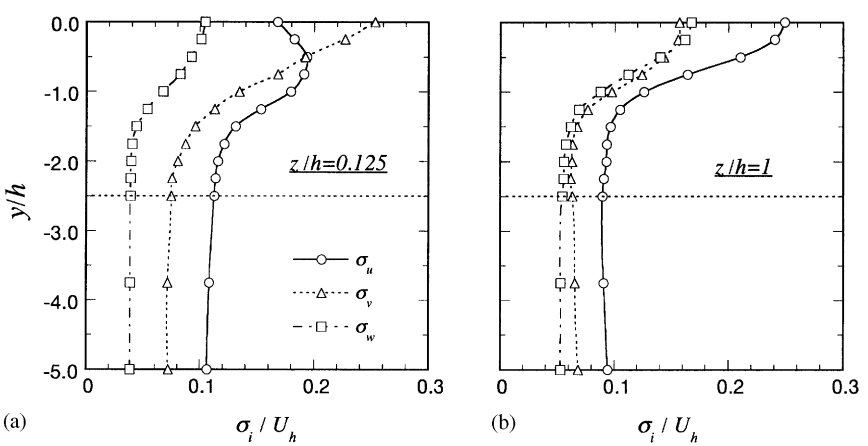

Fig. 10. Lateral distributions of three normal stress components behind the hill at (a) $x/h = 3.75$, $z/h = 0.125$ and (b) $x/h = 3.75$, $z/h = 1$.

values at the central position, and decay with distance away from the center line. In the region near the surface, the normal stresses behave in quite different ways. In particular, the longitudinal component σ_u displays a broad peak at a clearly off-center position, corresponding to maximum shear in the lateral profiles of U. The other remarkable behavior is that a peak in σ_v is observed at the central position. The peaks are also observed in the profile of the lateral component σ_v at the leeward hill foot at $x/h = 2.5$, as shown in Fig. 10. This similar result implies that in the wall layer behind the hill, there are coherent motions in the spanwise direction.

3.4. Spectra

In the three-dimensional wake, points of inflexion for the mean velocity U occur not only in the vertical profiles, but also in the lateral distributions. They generally cause some flow instabilities, such as vortex shedding. Spectral analysis may shed some light on the dynamics of the eddy motions in the near-wake region.

Fig. 11 plots normalized velocity spectra from measurements at the position $x/h = 3.75$ on the central plane of the hill. These spectra have been calculated by the

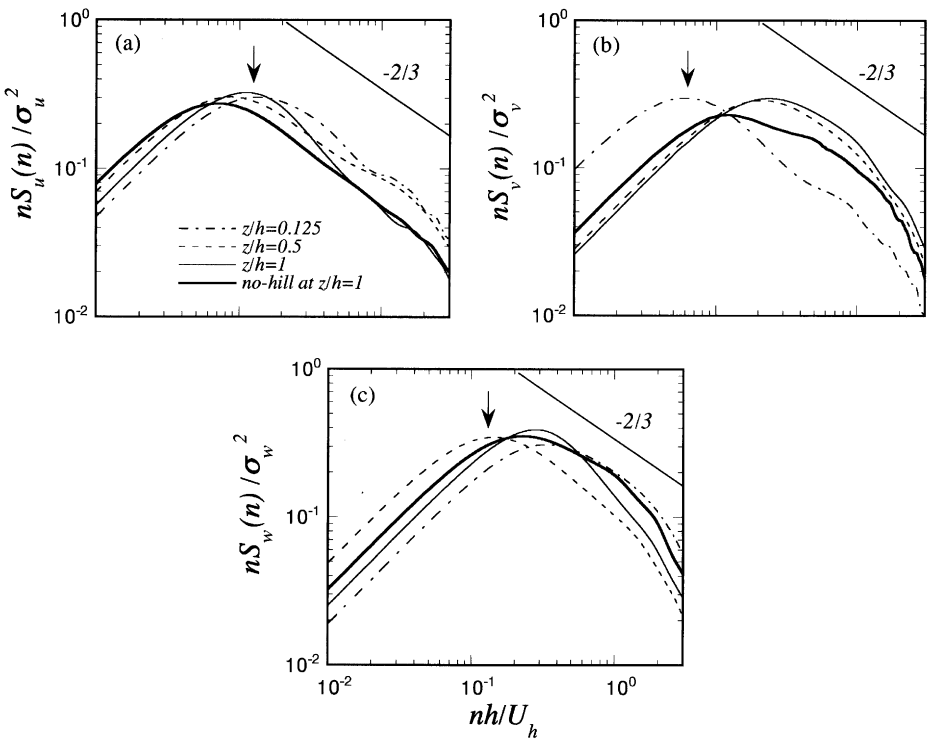

Fig. 11. Normalized velocity spectra from measurements at the position $x/h = 3.75$ on the central plane: (a) u component; (b) v component; (c) w component.

maximum-entropy method (MEM) and normalized by the standard deviations of fluctuating velocities. The abscissa represents a non-dimensional frequency, where n is the natural frequency in Hz. The spectra obtained at the height of $z/h = 1$ in the undisturbed boundary layer are also drawn in the figures as a reference data.

The u spectra at three heights shown in Fig. 11a display a $-\frac{2}{3}$ slope in the inertial subrange, predicted by Kolmogorov's hypothesis. Comparing the reference data, however, the data at $z/h = 1$ has a broad peak at the frequency $nh/U_h = 0.13$. It is reasonable to assume that this peak of the spectra corresponds to the shedding of vortices from the separation bubble.

The v spectra at three heights shown in Fig. 11b correspond approximately to the $-\frac{2}{3}$ slope in the inertial subrange. It should be noticed that an evident peak at $nh/U_h = 0.065$ appears on the data at $z/h = 0.125$, and has half of the frequency observed on the u spectra at $z/h = 1$. This result indicates that there are low-frequency motions in the wall layer behind the hill. The constant σ_u layer observed in the wall layer can be interpreted as a result of the horizontal mixing due to these motions. At $z/h \geqslant 0.5$, however, the data show a shift towards a higher frequency peak, indicating that the scale in the spanwise direction of vortices shed from the separation bubble behind the crest of the hill is smaller than that in the streamwise direction.

A broad peak at the frequency $nh/U_h = 0.13$ is also observed in the w spectra at $z/h = 0.5$. The result corresponds to the fact that σ_w shows a maximum at $z/h = 0.5$. The vortex shed from the separation bubble may be inclined downward due to the descending flow behind the hill. Besides the data at $z/h = 0.5$, the w spectra show a shift towards a higher frequency peak.

4. Conclusions

The results of split-fiber measurements of flow over a circular hill with a maximum slope of about 32° have brought out several interesting features. The pronounced speed-up of flow occurs not only at the hilltop but also at the midway slope on its side. The flow behind the steep, circular hill is characterized by the occurrence of a separation flow in the lee slope, reattaching just at the lee foot, and a low-frequency motion in the wall layer beyond the hill. The maximum perturbations in the longitudinal and vertical velocity variances were observed around the height of $z/h = 1$, corresponding to the separated recirculating flow, while the maximum in the lateral velocity variance appeared at the height of $z/h = 0.125$ beyond the hill, corresponding to the low-frequency motion in the wall layer.

References

[1] P.A. Taylor, P.J. Mason, E.F. Bradley, Boundary-layer over low hills – a review, Boundary- Layer Meteorol 39 (1987) 107–132.

[2] J.J. Finnigan, Air flow over complex terrain, in: W.L. Steffen, O.T. Denmead (Eds.), Flow and Transport in the Natural Environment, Springer, Berlin, 1988, pp. 183–229.

[3] E.F. Bradley, An experimental study of the profile of wind speed, shearing stress and turbulence at the crest of a large hill, Quart. J. Roy. Meteorol. Soc. 106 (1980) 101–124.
[4] P.J. Mason, J.C. King, Measurements and predictions of flow and turbulence over an isolated hill of moderate slope, Quart. J. Roy. Meteorol. Soc. 111 (1985) 617–640.
[5] I.P. Castro, W.H. Snyder, A wind tunnel study of dispersion from sources downwind of three-dimensional hills, Atmos. Environ. 16 (1982) 1869–1887.
[6] J.R. Pearse, Wind flow over conical hills in a simulated atmospheric boundary layer, J. Wind Eng. Indus. Aerodyn. 10 (1982) 303–313.
[7] S.P.S. Arya, P.S. Gadiyaram, An experimental study of flow and dispersion in the wakes of three-dimensional low hills, Atmos. Environ. 20 (1986) 729–740.
[8] W. Gong, A. Ibbetson, A wind tunnel study of turbulence flow over model hills, Boundary-Layer Meteorol. 49 (1989) 113–148.
[9] N.K. Tutu, R. Chevray, Cross-wire anemometry in high intensity turbulence, J. Fluid Mech. 71 (1975) 785–800.
[10] M. Kiya, K. Sasaki, Structure of a turbulent separation bubble, J. Fluid Mech. 137 (1983) 83–113.
[11] K. Sasaki, M. Kiya, Turbulence measurements in a reverse flow region by means of split-film probe, J. JSME B 51 (1985) 1615–1618 (in Japanese).
[12] T. Boerner, H.J. Leutheusser, Calibration of split-fiber probe for use in bubbly two-phase flow, DISA Info., No. 29, 1984, pp. 10–13.
[13] T. Ishihara, K. Hibi, Turbulence characteristics and organized motions on the flat roof of a high-rise building, J. Wing Eng. 72 (1997) 21–34 (in Japanese).
[14] J. Counihan, Adiabatic atmospheric boundary layers: a review and analysis of data from the period 1880–1972, Atmos. Environ. 9 (1975) 871–905.
[15] J.C.R. Hunt, W.H. Snyder, Experiments on stably and neutrally stratified flow over a model three-dimensional hill, J. Fluid Mech. 96 (1980) 704–761.
[16] I.P. Castro, A. Haque, The structure of turbulent shear layer bounding a separation region, J. Fluid Mech. 179 (1987) 439–468.
[17] N. Itoh, N. Kasagi, Turbulence measurement in a separated and reattaching flow over a backward-facing step with the three-dimensional particle tracking velocimeter, J. Flow Visualization Soc. Jpn. 9 (34) (1989) 245–248 (in Japanese).